The 2009 IEEE/RSJ International Conference on
Intelligent Robots and Systems
October 11-15, 2009 St. Louis, USA

Micromanipulation Using Artificial Bacterial Flagella

Li Zhang, Jake J. Abbott, Lixin Dong, Bradley E. Kratochvil,
Haixin Zhang, Kathrin E. Peyer, and Bradley J. Nelson

***Abstract*—Artificial bacterial flagella (ABF) are swimming microrobots that mimic the swimming motion of bacteria. The helical swimmer consists of an InGaAs/GaAs/Cr helical nanobelt tail fabricated by a self-scrolling technique with dimensions similar to a natural flagellum, and a thin soft-magnetic metal "head" consisting of a Cr/Ni/Au multi-layer. The swimming locomotion of ABF is precisely controlled in 3-D by external rotating magnetic fields. Microsphere manipulation is performed by ABF, and experimental results show that both the position and the orientation of microspheres can be precisely controlled. The propelling force of ABF is in the pico-Newton range. We also describe a swarm-like behavior in which three ABF swim in a pack, indicating the potential to handle several micro objects in parallel. Self-propelled devices such as these are candidates for wireless 6-DOF micro and nanomanipulation tools for handling cellular and sub-cellular objects.**

I. Introduction

The controlled locomotion of untethered microrobots in a liquid environment is of interest for both fundamental research and biomedical applications. Previous work has shown that the use of external magnetic fields for propelling millimeter and micrometer scale robotic agents in liquid via wireless energy transfer is effective [1-6]. However, all these artificial agents are still several orders-of-magnitude larger than natural microscopic organisms such as bacteria. In 1973, Berg *et al.* discovered that bacteria, such as Escherichia Coli, swim in liquid by rotating their flagella filaments in a bundle [7]. Flagellar mechanisms are particularly well suited to the low-Reynolds-number environment in which they live because of their ability to generate non-reciprocating motion [8, 9]. Inspired by monotrichous bacteria flagella, we have fabricated artificial bacterial flagella (ABF) that have comparable geometries and dimensions to their organic counterparts and can swim in a controllable fashion using weak applied magnetic fields [10]. ABF swimmers represent the first demonstration of microscopic artificial swimmers that use helical propulsion, and are many orders of magnitude smaller than any existing artificial helical swimmers [2, 11].

Self-propelled devices such as ABF [10] can provide a 6-DOF micro- and nanomanipulation tool for manipulating cellular or sub-cellular objects. Typical manipulation tasks that ABF have the potential to perform are shown schematically in Fig. 1. The screwing motion of ABF can be used for (a) pushing, (b) twisting, or (c) rotating an object based on its size and shape. The helical structure of ABF can be used for (d) pumping. For biomedical applications, ABF can potentially be used for (e) drilling through the membrane of a cell for sampling, sensing, (f) drug delivery, or (g) injection. Magnetic approaches have the advantage that they do not require high-intensity lasers [12] or a special environment of a particular chemical composition that serves as a fuel [13-15].

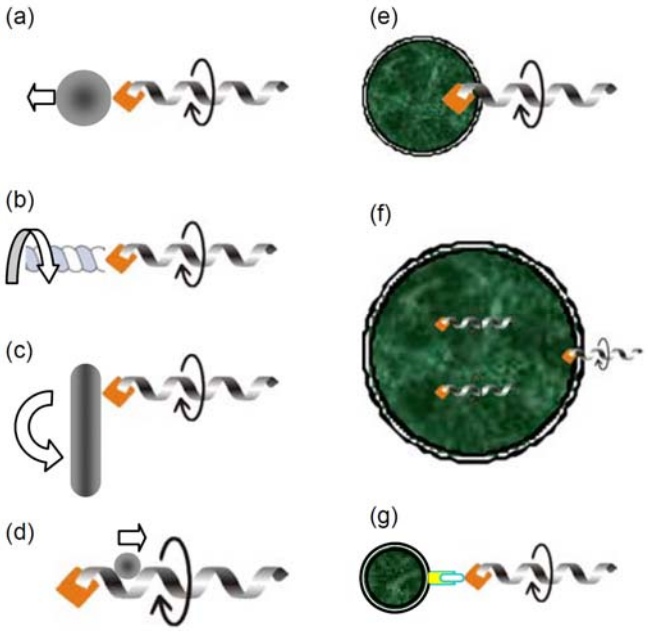

Fig. 1: Typical manipulation processes using artificial bacterial flagella. (a) Pushing, (b) Twisting, (c) Rotating, (d) Pumping, (e) Drilling, (f) Drug delivery, and (g) Injecting.

II. Fabrication

An artificial bacterial flagellum developed as a micro-device capable of controlled untethered locomotion in liquid consists of two parts: a helical nanobelt tail resembling a natural flagellum in both size and shape and a soft-magnetic head in the shape of a thin square plate. Fig. 2 shows a field emission scanning electron microscopy (FESEM) micrograph of an as-fabricated ABF. We use the terms "tail" and "head" loosely, as the ABF swimmers have no preferred forward orientation.

This work is supported in part by the Swiss National Science Foundation (SNSF).

The authors are with the Multi-Scale Robotics Lab, Institute of Robotics and Intelligent Systems, ETH Zurich, CH-8092 Zurich, Switzerland. J. J. Abbott is now with the Department of Mechanical Engineering, University of Utah, Salt Lake City, Utah 84112, USA. L. X. Dong is now with the Department of Electrical and Computer Engineering, Michigan State University, East Lansing, Michigan 48824, USA. B. J. Nelson is the corresponding author. bnelson@ethz.ch

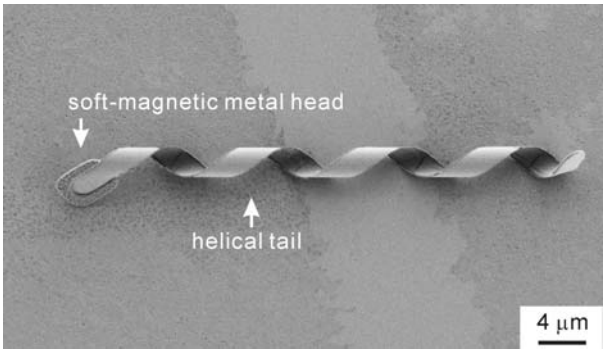

Fig. 2: FESEM image of an untethered artificial bacterial flagellum that consists of a soft-magnetic metal head and a helical tail. The ribbon width and the diameter of the helical tail are 1.8 μm and 2.8 μm, respectively. The metal head is a thin square Cr/Ni/Au plate.

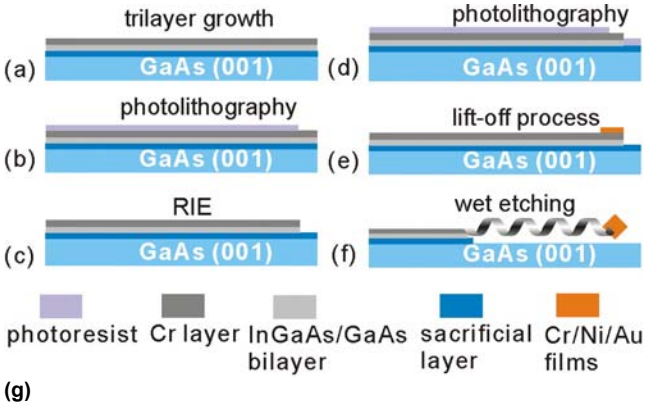

Fig. 3: (a–f) Fabrication procedure of the ABF with InGaAs/GaAs/Cr helical tail. (g) The chirality, helicity, and pitch of a helix is determined by the scrolling direction of the ribbon, with $\lambda = 2\pi r \tan \theta$.

The fabrication of the ABF is based on a self-scrolling technique [16-19]. First, an AlGaAs sacrificial layer and an InGaAs/GaAs bilayer are epi-grown on a GaAs (001) wafer by molecular beam epitaxy (MBE). After the deposition of a 15 nm Cr layer by e-beam evaporation, the InGaAs/GaAs/Cr trilayer is patterned into a ribbon-like mesa for the tail by reactive ion etching (RIE). Then, the soft-magnetic metal head is prepared by e-beam evaporation of Cr/Ni/Au thin films and a lift-off process. Finally, the AlGaAs sacrificial layer is selectively etched by 2% HF aqueous solution to release the patterned mesa on which the 2-D patterned films self-organize into a helix to form an artificial bacteria flagellum as shown in Fig. 3(a-f). For the experiments, the InGaAs/GaAs/Cr trilayer has a thickness of 11/16/15 nm, the ribbon width is 1.8 μm, and the diameter of the as-fabricated

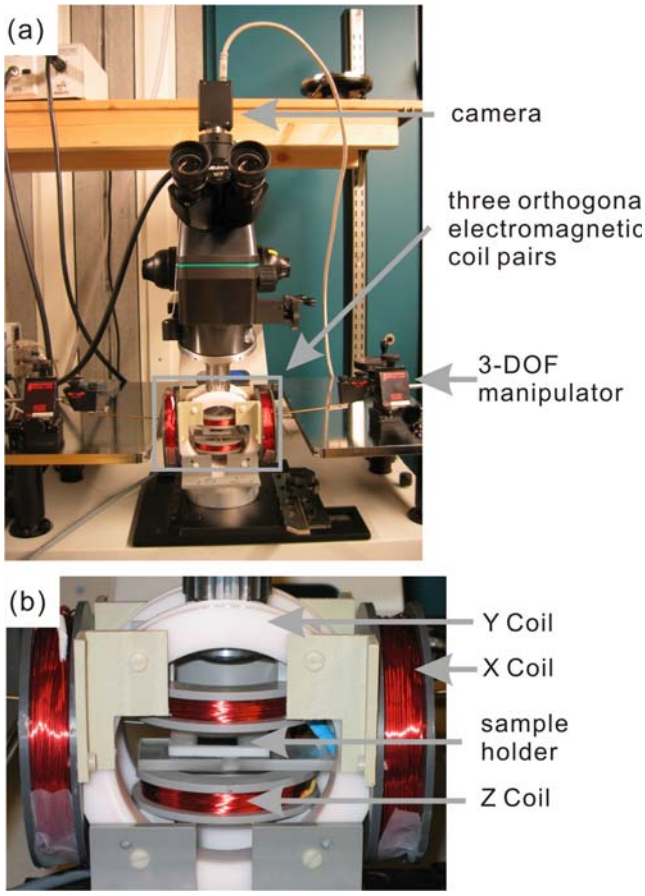

Fig. 4: (a) The experimental setup for the ABF swimming tests using three orthogonal pairs of electromagnetic coils. (b) Close-up view of the coils. The sample holder is placed at the center of the coils.

ABF is 2.8 μm. Different materials are candidates for helical tail fabrication, including semiconductors, metals, and polymers [17, 20-23]. The soft-magnetic metal head is in the shape of a thin square plate with dimensions of 4.5 μm (length) × 4.5 μm (width) × 200 nm (thickness). It is composed of a Cr/Ni/Au trilayer with a thickness of 10/180/10 nm, respectively. Since the helix is rolled up from a ribbon, the chirality, the helicity angle, and the pitch of a helix is determined by the misalignment angle between the scrolling direction and the orientation of the ribbon as shown in Fig. 3(g). The diameter of the helical tail can also be controlled as reported previously [18, 19, 24].

By fabricating the head as a thin square plate that is rectilinearly aligned with the ribbon, and then controlling the pitch of the helix to 45°, we ensure that one diagonal of the square plate is perpendicular to the helix axis after self-scrolling, as shown in Fig. 2. In Section IV we explain how this head geometry is exploited in ABF propulsion and steering. Because we make use of soft-magnetic materials, no magnetization is required in the fabrication process. We also found that preparing helical tails with the Cr deposition step makes them less fragile for the manipulation step required to cut, pick, and place the ABF in liquid.

III. Experimental Setup

For precise control of the motion of the ABF under an optical microscope, three orthogonal electromagnetic coil pairs were constructed to generate a uniform rotating magnetic field. The experimental setup is shown in Fig. 4. Our setup requires no special modification of the probe station (Signatone model S-1160); the coils are simply placed around the lens. The parameters of the three coil pairs are presented in Table I. The power amplifiers (Maxon Motor Control 4-Q-DC Servoamplifier LSC 30/2) have a maximum output voltage of 24V and maximum output current of 2 A. During the experiments, a maximum field of 2.0 mT is generated. A CMOS camera is connected to the control PC for 30 fps (frame-per-second) video recording of the microscope images.

To untether the ABF from the substrate, micromanipulation was performed *in situ* in the following way: first, an ABF is cut from the substrate using a tungsten probe mounted on a manipulator (Signatone model S-926) under the optical microscope. The radius of the probe tip is 100 nm. Due to van der Waals forces, the ABF sticks to the probe. Next, the ABF is transferred from the GaAs surface by moving the manipulator probe above a Si wafer coated by SiO_2. The ABF is released by tapping the manipulator. Finally, a rotating magnetic field is applied to drive the ABF away from the probe. The reservoir for swimming experiments has a dimension of 20mm (length) × 15mm (width) × 2mm (depth), and the sample is always immersed in deionized water with a viscosity of 1mPa·s.

Using three orthogonal coil pairs, we can set the three components of the magnetic field vector **B** independently, which are directly proportional to the amount of current through each coil pair. The vector **B** consists of the field magnitude at time t, i.e. b_t, and a unit vector pointing along the y-axis in the desired robot frame,

$$B_t = b_t \begin{bmatrix} 0 \\ 1 \\ 0 \end{bmatrix} \tag{1}$$

which is described with respect to the world frame by the rotation matrix R_t. When moving the helical swimmer, the field's rotational velocity is controlled by the scalar value ω in Hz. The field simply rotates around the desired microrobot coordinate frame's x-axis as described by:

$$\xi_\omega = 2\pi\omega_t \begin{bmatrix} 1 \\ 0 \\ 0 \end{bmatrix} \tag{2}$$

$$R_{t+\Delta t} = R_t e^{\hat{\xi}_\omega \Delta t} \tag{3}$$

where the $\hat{}$ operator converts a vector into its skew-symmetric matrix representation, and Δt represents the size of the discrete time step during the experiment. We make use of the product-of-exponentials formulation of robotics in order to avoid representational singularities in the control of our fully untethered microrobots [25]. In order to steer the robot in a desired direction, we must take into consideration additional transformation matrices that describe the desired microrobot orientation in the world coordinate frame. We are restricted to control parameters β and γ, which describe the device's desired yaw and pitch at time t, as expressed by equations:

TABLE I
THE PARAMETERS OF THE THREE ELECTROMAGNETIC COIL PAIRS (TWO COILS CONNECTED IN SERIES)

	X Coils	Y Coils	Z Coils
measured mean diameter (mm)	65	92	61
measured mean separation (mm)	127	55	34
wire size (mm)	0.75	0.35	0.35
total number of wraps	900	1000	640
measured resistance (Ω)	8.0	73	31
measured inductance (mH)	29	82	21
measured field/current (mT/A)	1.8	8.5	8.7

$$\xi_\beta = \beta_t \begin{bmatrix} 0 \\ 1 \\ 0 \end{bmatrix} \tag{4}$$

$$\xi_\gamma = \gamma_t \begin{bmatrix} 0 \\ 0 \\ 1 \end{bmatrix} \tag{5}$$

$$B = e^{\hat{\xi}_\beta} e^{\hat{\xi}_\gamma} R_{t+\Delta t} B_t \tag{6}$$

In the user interface, pitch is the angle of the ABF helix axis with respect to the horizontal plane, and yaw is the angle of the ABF helix axis observed in the horizontal imaging plane. Thus, in total, the user is able to control the robots using four scalar values: b_t in T, ω_t in Hz, β_t and γ_t in rad.

IV. Wireless Control of ABF

A. Magnetic propulsion

To steer an ABF in fluid in 3-D, the orientation vector and rotation frequency are independently controlled in software. For forward and backward motion the ABF acts as a helical propeller to convert rotary motion to linear motion as shown in Fig. 5(a-b), thus, forward and backward motion can be switched by simply reversing the rotation direction. By rotating the magnetic field clockwise (with an observer in front of the ABF), a left-handed ABF swims forward, and by rotating the field counterclockwise it moves backward. The magnetic torque for rotation is generated by the thin head attempting to align with the applied field as shown in Fig. 5(c-d). In Fig. 5(e) a series of frames of an ABF, which has a left-handed chirality and a tail length of 47 μm, swims forward by rotating the magnet field clockwise (as seen by an observer in front of the ABF) until t = 8 sec, then the ABF reverses direction by rotating the field counterclockwise.

In contrast to reversing motion by turning the swimmer 180°, which is the method used by bacteria and existing microscopic artificial swimmers [6], reversing the rotation

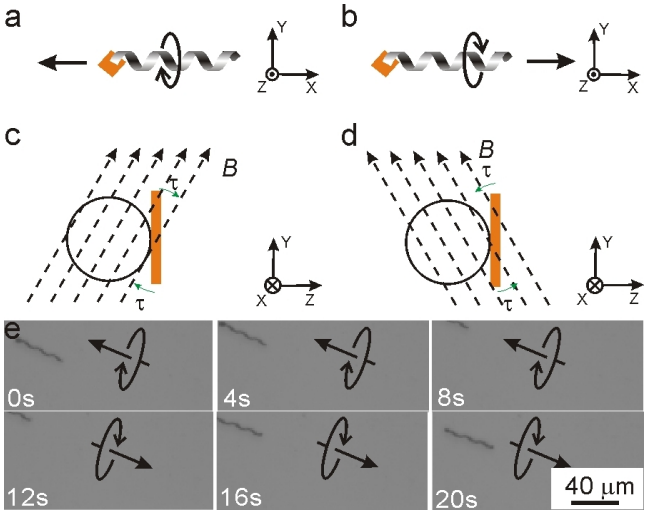

Fig. 5: An ABF swimmer is propelled by magnetic fields. (a-d) Schematic of a left-handed ABF swimming forward and backward. With the field B continuously rotating perpendicular to the X axis of the ABF, a misalignment angle between the field and the thin magnetic head will induce a magnetic torque (τ) that attempts to align the ABF head with the field, resulting in rotation and propulsion of the ABF. Note that the X-Y-Z coordinates are correlative to the X, Y, and Z coils in Fig. 4 and Table I. (e) Optical microscope images of the forward/backward motion of an ABF controlled by magnetic fields. The commanded translation and rotation directions of the ABF are indicated by the arrows.

direction is a more straightforward and time-efficient method, especially for use as a micromanipulation tool.

B. *Magnetic steering*

In addition to a magnetic torque for propulsion, there is a magnetic torque used for steering. It has been reported that in a weak applied field the easy magnetization axes of a thin square plate are along the diagonals [26]. It is also known that magnetic torque will tend to align an easy axis with the applied field. Although there are two possible easy axes in a square plate (i.e., *ac* and *bd* in Fig. 6(a-b)), the one that is closer to the applied field will act as the easy axis (i.e., *ac* in Fig. 6(a) and *bd* in Fig. 6(b)). We ensure that the diagonal *ac*, which is perpendicular to the axis of the ABF helix, becomes the magnetized axis during normal swimming. When the magnetic field is misaligned by less than 45° with respect to this easy axis (i.e., $\gamma < 45°$ in Fig. 6(a)), the magnetic head will attempt to align to the external field as the helix rotates axially. Figure 6(c) shows a series of an ABF turning 80° in 6 seconds with propulsion. When the other diagonal is closer to the magnetic field (i.e., $\gamma < 45°$ in Fig. 6(b)), that diagonal will become the magnetized axis, and the ABF will attempt to rotate perpendicular to the helix axis, which is undesirable during swimming but is useful for orienting a stationary ABF. Figure 6(d) shows a stationary ABF steered in this mode, in which the ABF rotates a half-turn in 1 second. In the experiment, the applied magnetic fields have a rotational frequency of 0.5 Hz, thus the ABF rotates synchronously.

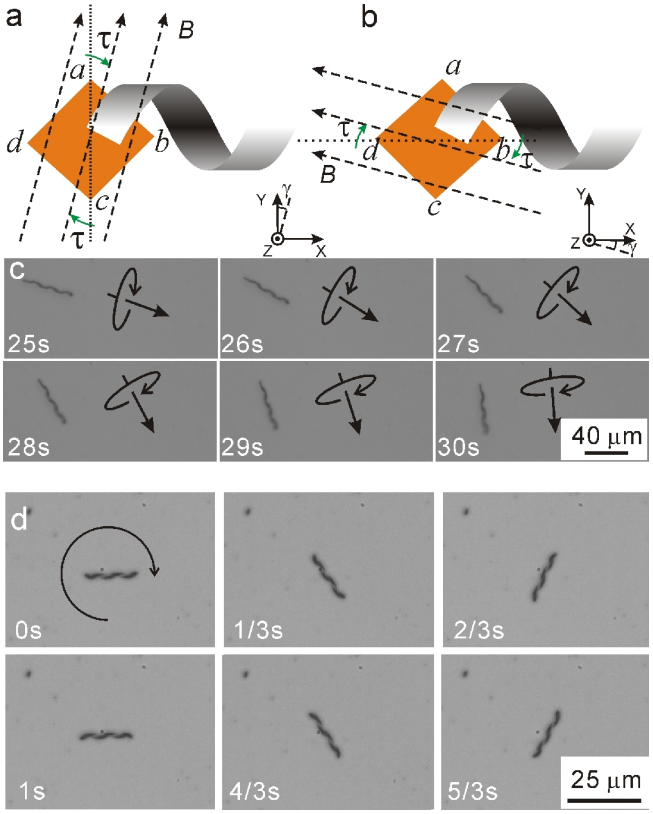

Fig. 6: (a) If the field is rotated about the Y axis by an angle $\gamma < 45°$ with respect to the easy axis *ac* of the head, then the ABF is steered an angle γ as it is propelled as the easy axis *ac* attempts to align with the field. This is the steering principle used during normal operation of the ABF. (b) If the field is rotated about the X axis by an angle $\gamma < 45°$ with respect to the easy axis *bd*, the ABF will instantaneously attempt to rotate perpendicular to the helix axis. However, steering using the *bd* easy axis is not simultaneously possible with forward/backward propulsion. (c) Optical microscope images of the turning motion of an ABF controlled by magnetic fields. The commanded translation and rotation directions of the ABF are indicated by the arrows. (d) Pure rotational motion of the ABF with frequency of 0.5 Hz (see text). The arrow indicates the rotation direction.

C. *Swimming motion in 3-D*

Although inertial effects of ABF are negligible and ABF reach their steady-state velocities in water nearly instantaneously, the weight of an ABF must be taken into account for swimming [27]. To avoid the ABF sinking toward the substrate due to gravity, it is necessary to keep the ABF swimming with a positive pitch angle. A further advantage of swimming with a positive pitch angle is to minimize the interaction between the ABF and the substrate due to, e.g., van der Waals force. Thus, a small pitch angle (10°–20°) is applied in the experiments when the ABF swim near a wall. Figure 7(a) illustrates turning of an ABF away from the horizontal plane until the helical axis of the ABF becomes parallel to the Z-axis (vertical). Figure 7(b) shows a series of frames of an ABF steered from the horizontal plane to the Z-axis.

ABF do not swim upwards with a positive pitch angle unless propulsion speed along the Z-axis reaches a value that

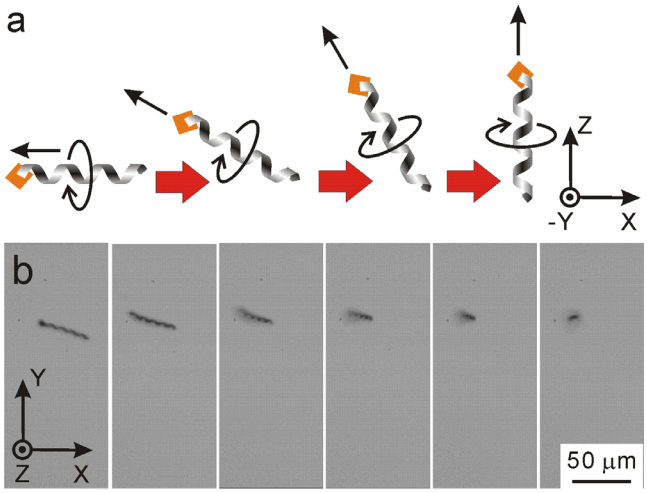

Fig. 7: (a) The ABF is steered from the horizontal plane (X-Y plane) to the vertical Z axis. The commanded translation and rotation directions of the ABF are indicated by arrows. (b) Optical microscope images shows the ABF turning from the horizontal plane controlled by magnetic fields.

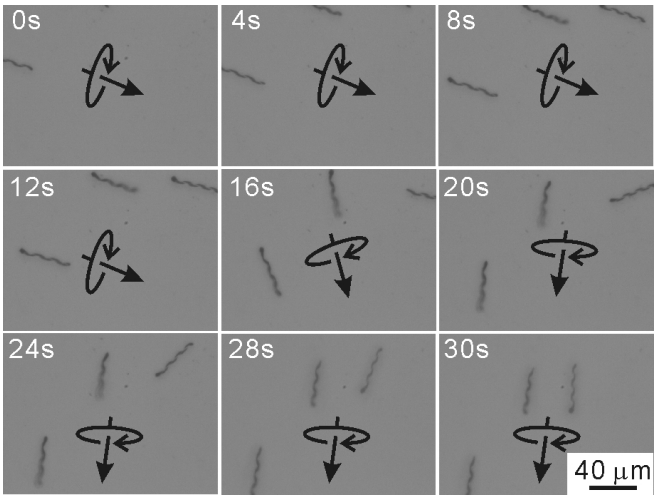

Fig. 9: (a) Swarm-like behavior of three ABF controlled by magnetic fields. The swarm is controlled as a single entity, with the commanded translation and rotation directions of the field indicated by the arrows. During a relatively fast steering movement, one ABF swimmer is temporarily separated from the swarm, but it naturally rejoins.

generates enough propulsion force to overcome the weight of the ABF. A simple test was performed to validate that ABF can swim in 3-D. First, an ABF is placed on a Si substrate and then swims into free space where a wall boundary is not nearby. Then, we steer the ABF back to the Si substrate by only changing the yaw value as shown in Fig. 8. The results show that if a 4.5 turn ABF has a minimum rotating frequency of 10 Hz with a pitch angle of 25°, its weight will not prevent swimming in 3-D.

D. Swarm-like behavior

In addition to the experiments that characterize single ABF, we have demonstrated a simple swarm-like behavior in which three ABF swim in a coordinated fashion, as shown in Fig. 9. We find that the swarm can be easily controlled as a single entity, and that ABF swimmers that get temporarily separated from the swarm due to steering maneuvers naturally return to the swarm. From Fig. 9 it can be seen that although one of the ABF was unable to follow one of the commanded steering directions (probably due to a fast steering command and small inhomogeneities in the magnetic field), it eventually rotates into alignment and swims in the same direction as the other two swimmers.

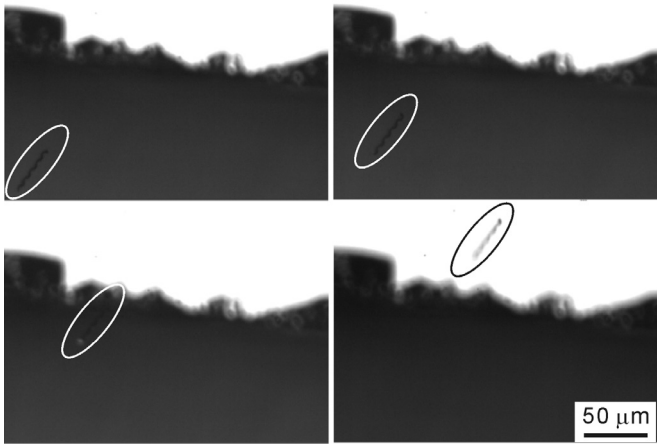

Fig. 8: (a) An ABF swims from free space to a Si substrate. Since there is no reflection of light in free space, the brightness is low; the Si surface has high brightness due to strong light reflection. The ABF is indicated by the ellipse.

V. Micromanipulation of Microspheres Using ABF

Fig. 10 demonstrates two basic manipulation tasks using an ABF, i.e. translation and rotation of microspheres. In Fig. 10 (a), the image sequence shows an ABF pushing on one of two connected 6-μm-diameter polystyrene microspheres (Polysciences Inc.). The ABF is not rigidly connected to the microsphere, but rather, swims toward it under human guided control. The image sequence shows that the ABF is able to rotate the connected microspheres 70° in 2 seconds. To estimate the thrust force of the ABF, a single microsphere was pushed (Fig. 10(b)). Results show that the microsphere has a translational velocity of 3 μm/s when the angular speed of the ABF is 31.4 rad/s. In this low-Reynold-number regime, the thrust force of the ABF is counterbalanced by the drag force of the microsphere in water, and the drag force of a sphere is expressed as [28]:

$$F_{thrust} = F_{drag} = 3\pi\eta dv \qquad (7)$$

in which η is the viscosity of the water, and d and v are the diameter and velocity of the microsphere, respectively. Thus the propulsive force of the ABF is calculated as 0.17 pN with an angular speed of 31.4 rad/s, which is similar to that of state-of-the-art nanowire-based swimmers immersed in H_2O_2 that serves as a fuel source [13, 14]. However, in contrast to the nanowire-based swimmers, the propulsive force of ABF swimmer can be tuned in a controllable fashion by changing the angular speed of the ABF. And, just as significantly, the swimming takes place in H_2O rather than H_2O_2.

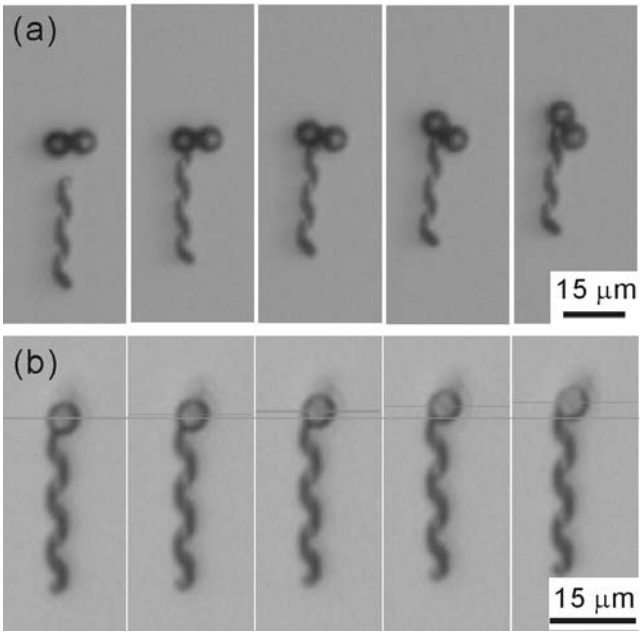

Fig. 10: (a) Two polystyrene microspheres are rotated 70° by a 29 μm long InGaAs/GaAs/Cr ABF pushing on one of the microspheres. The optical-microscope image sequence represents two seconds of elapsed time. (b) The microsphere is pushed for a radius length by the ABF within one second.

VI. Conclusions

In conclusion, ABF are untethered swimming microrobots that mimic bacterial flagella in both dimension and motion. The swimmer consists of an InGaAs/GaAs/Cr helical tail and a thin soft-magnetic metal "head." Experimental investigation has shown that ABF can be propelled and steered precisely in 3-D in water by a low-strength, rotating magnetic field. These helical swimming microrobots can manipulate microspheres for translation and rotation. These magnetically driven helical devices can be used as wireless manipulators for medical and biological applications under 3-D control in fluid environments, and have the potential to perform micro and nano manipulation with a full six degrees of freedom.

Acknowledgment

The authors thank the FIRST Lab of ETH Zurich for technical support.

References

[1] G. T. Gillies, R. C. Ritter, W. C. Broaddus, M. S. Grady, M. A. Howard, and R. G. Mcneil, "Magnetic Manipulation Instrumentation for Medical Physics Research," *Rev. Sci. Instrum.* vol. 65, pp. 533-562, 1994.

[2] T. Honda, K. I. Arai, and K. Ishiyama, "Micro swimming mechanisms propelled by external magnetic fields," *IEEE Trans. Magn.* vol. 32, pp. 5085-5087, 1996.

[3] M. B. Khamesee, N. Kato, Y. Nomura, and T. Nakamura, "Design and control of a microrobotic system using magnetic levitation," *IEEE-ASME Trans. Mechatron.* vol. 7, pp. 1-14, 2002.

[4] A. Yamazaki, M. Sendoh, K. Ishiyama, K. I. Arai, R. Kato, M. Nakano, and H. Fukunaga, "Wireless micro swimming machine with magnetic thin film," *J. Magn. Magn. Mater.* vol. 272, pp. E1741-E1742, 2004.

[5] K. B. Yesin, K. Vollmers, and B. J. Nelson, "Modeling and control of untethered biomicrorobots in a fluidic environment using electromagnetic fields," *Int. J. Robot. Res.* vol. 25, pp. 527-536, 2006.

[6] R. Dreyfus, J. Baudry, M. L. Roper, M. Fermigier, H. A. Stone, and J. Bibette, "Microscopic artificial swimmers," *Nature* vol. 437, pp. 862-865, 2005.

[7] H. C. Berg and R. A. Anderson, "Bacteria Swim by Rotating their Flagellar Filaments," *Nature* vol. 245, pp. 380-382, 1973.

[8] E. M. Purcell, "Life at Low Reynolds-Number," *Am. J. Phys.* vol. 45, pp. 3-11, 1977.

[9] D. C. Rapaport, "Microscale swimming: The molecular dynamics approach," *Phys. Rev. Lett.* vol. 99, 2007.

[10] K. Ishiyama, K. I. Arai, M. Sendoh, and A. Yamazaki, "Spiral-type micro-machine for medical applications," *J. Micromechatronics* vol. 2, pp. 77-86, 2003.

[11] L. Zhang, J. J. Abbott, L. X. Dong, B. E. Kratochvil, D.J. Bell and B. J. Nelson, "Artificial Bacterial Flagella: Fabrication and Magnetic Control" *Appl. Phys. Lett.*, vol. 94, pp. 064107, 2009.

[12] A. Ashkin and J. M. Dziedzic, "Optical Trapping and Manipulation of Viruses and Bacteria," *Science* vol. 235, pp. 1517-1520, 1987.

[13] J. Burdick, R. Laocharoensuk, P. M. Wheat, J. D. Posner, and J. Wang, "Synthetic nanomotors in microchannel networks: Directional microchip motion and controlled manipulation of cargo," *J. Am. Chem. Soc.* vol. 130, pp. 8164-8165, 2008.

[14] S. Sundararajan, P. E. Lammert, A. W. Zudans, V. H. Crespi, and A. Sen, "Catalytic motors for transport of colloidal cargo," *Nano Lett.* vol. 8, pp. 1271-1276, 2008.

[15] J. Wang, "Can Man-Made Nanomachines Compete with Nature Biomotors? ,"*ACS NANO* vol. 3, pp. 4-9, 2009.

[16] V. Y. Prinz, V. A. Seleznev, A. K. Gutakovsky, A. V. Chehovskiy, V. V. Preobrazhenskii, M. A. Putyato, and T. A. Gavrilova, "Free-standing and overgrown InGaAs/GaAs nanotubes, nanohelices and their arrays," *Physica E* vol. 6, pp. 828-831, 2000.

[17] O. G. Schmidt and K. Eberl, "Nanotechnology - Thin solid films roll up into nanotubes," *Nature* vol. 410, pp. 168-168, 2001.

[18] L. Zhang, E. Deckhardt, A. Weber, C. Schonenberger, and D. Grutzmacher, "Controllable fabrication of SiGe/Si and SiGe/Si/Cr helical nanobelts," *Nanotechnology* vol. 16, pp. 655-663, 2005.

[19] L. Zhang, E. Ruh, D. Grutzmacher, L. X. Dong, D. J. Bell, B. J. Nelson, and C. Schonenberger, "Anomalous coiling of SiGe/Si and SiGe/Si/Cr helical nanobelts," *Nano Lett.* vol. 6, pp. 1311-1317, 2006.

[20] O. G. Schmidt, N. Schmarje, C. Deneke, C. Muller, and N. Y. Jin-Phillipp, "Three-dimensional nano-objects evolving from a two-dimensional layer technology," *Adv. Mater.* vol. 13, pp. 756-759, 2001.

[21] A. Cho, "Pretty as You Please, Curling Films Turn Themselves Into Nanodevices," *Science* vol. 313, pp. 164-165, 2006.

[22] V. Luchnikov, M. Stamm, C. Akhmadaliev, L. Bischoff, and B. Schmidt, "Focused-ion-beam-assisted fabrication of polymer rolled-up microtubes," *J. Micromech. Microeng.* vol. 16, pp. 1602-1605, 2006.

[23] L. Zhang, L. X. Dong, and B. J. Nelson, "Ring closure of Rolled-up Si/Cr Nanoribbons," *Appl. Phys. Lett.* vol. 92, p. 143110, 2008.

[24] D. J. Bell, L. X. Dong, B. J. Nelson, M. Golling, L. Zhang, and D. Grutzmacher, "Fabrication and Characterization of Three-dimensional InGaAs/GaAs Nanosprings," *Nano Lett.* vol. 6, pp. 725-729, 2006.

[25] R. M. Murray, Z. Li, and S. S. Sastry, *A Mathematical Introduction to Robotic Manipulation*. Boca Raton, Florida: CRC Press, 1994.

[26] F. B. Hagedorn and E. M. Gyorgy, "Magnetic-shape Anisotropy in Polygonal Prisms," *J. Appl. Phys.* vol. 39, pp. 995-998, 1968.

[27] J. J. Abbott, K. E. Peyer, M. Cosentino Lagomarsino, L. Zhang, L. X. Dong, I. K. Kaliakatsos, and B. J. Nelson, "How should microrobots swim?," *Int. J. Robotics Research*, In Press.

[28] J. Happel and H. Brenner, *Low Reynolds number hydrodynamics*. Boston: Kluwer, 1983.